Revealing time-varying joint impedance with kernel-based regression and nonparametric decomposition

van de Ruit, Mark; Cavallo, Gaia; Lataire, John; van der Helm, Frans C.T.; Mugge, Winfred; van Wingerden, Jan Willem; Schouten, Alfred C.

DOI
10.1109/TCST.2018.2881664

Publication date
2018

Document Version
Final published version

Published in
IEEE Transactions on Control Systems Technology

Revealing Time-Varying Joint Impedance With Kernel-Based Regression and Nonparametric Decomposition

Mark van de Ruit, Gaia Cavallo, *Student Member, IEEE*, John Lataire, *Member, IEEE*, Frans C. T. van der Helm, Winfred Mugge, Jan-Willem van Wingerden, and Alfred C. Schouten

***Abstract*— During movements, humans continuously regulate their joint impedance to minimize control effort and optimize performance. Joint impedance describes the relationship between a joint's position and torque acting around the joint. Joint impedance varies with joint angle and muscle activation and differs from trial-to-trial due to inherent variability in the human control system. In this paper, a dedicated time-varying system identification (SI) framework is developed involving a parametric, kernel-based regression, and nonparametric, "skirt decomposition," SI method to monitor the time-varying joint impedance during a force task. Identification was performed on single trials and the estimators included little a priori assumptions regarding the underlying time-varying joint mechanics. During the experiments, six (human) participants used flexion of the wrist to apply a slow sinusoidal torque to the handle of a robotic manipulator, while receiving small position perturbations. Both methods revealed that the sinusoidal change in joint torque by activation of the wrist flexor muscles resulted in a sinusoidal time-varying joint stiffness and resonance frequency. A third-order differential equation allowed the parametric kernel-based estimator to explain on average 76% of the variance (range 52%–90%). The nonparametric skirt decomposition method could explain on average 84% of the variance (range 66%–91%). This paper presents a novel framework for identification of time-varying joint impedance by making use of linear time-varying models based on a single trial of data.**

***Index Terms*— Human motor control, joint impedance, system identification (SI), time-varying systems.**

Manuscript received December 28, 2017; revised June 15, 2018 and September 18, 2018; accepted October 31, 2018. Date of publication December 4, 2018; date of current version December 27, 2019. This work was supported in part by the European Research Council through the European Union's Seventh Framework Program (FP/2007–2013) ERC under Grant 291339, Project 4DEEG: A new tool to investigate the spatial and temporal activity patterns in the brain. The work of J. Lataire was supported in part by the Flemish Government through the Methusalem and in part by the Belgian Government through the Inter University Poles of Attraction (DYSCO) Program. Recommended by Associate Editor G. Mercere. *(Corresponding author: Mark van de Ruit.)*

M. van de Ruit, F. C. T. van der Helm, W. Mugge, and A. C. Schouten are with the Laboratory for Neuromuscular Control, Department of Biomechanical Engineering, Delft University of Technology, 2628CD Delft, The Netherlands (e-mail: m.l.vanderuit-1@tudelft.nl; f.c.t.vanderhelm@tudelft.nl; w.mugge@tudelft.nl; a.c.schouten@tudelft.nl).

J. Lataire and G. Cavallo are with the Department of ELEC, Vrije Universiteit Brussel, 1050 Brussels, Belgium (e-mail: john.lataire@vub.be; gaia.cavallo@vub.be)

J.-W. van Wingerden is with the Delft Center for Systems and Control, Delft University of Technology, 2628CD Delft, The Netherlands (e-mail: j.w.vanwingerden@tudelft.nl).

Color versions of one or more of the figures in this article are available online at http://ieeexplore.ieee.org.

Digital Object Identifier 10.1109/TCST.2018.2881664

I. Introduction

HUMANS are able to perform skillful movements despite challenging environmental circumstances or the presence of external disturbances. Information provided by the body's internal sensors (proprioceptors) and actions executed by the body's actuators (muscles) are used to achieve this. Hereby, humans can adapt the dynamics of their joints by regulating their intrinsic and reflexive joint properties [1]. Ensuring adequate task performance at all times, the controller of the human body, i.e., the central nervous system, follows the principles of optimality and control effort minimization [2].

System identification (SI) can be used to quantify properties of the human joints during posture and movement. For example, joint impedance, describing the joint's resistance to external disturbances, may be determined by relating joint position and torques in response to a mechanical perturbation [1], [3]–[9]. However, joint impedance is affected by many physiological and mechanical factors such as muscular fatigue [10], joint angle and muscle activation level [7]. Therefore, time-invariant SI techniques are only applicable when the system remains in a fixed operation point, i.e., there are only small changes in joint angle or muscle activation. When this is not the case, time-varying SI techniques allow studying changing joint impedance across time, e.g., as a function of joint angle or muscle activation level.

There are many SI techniques for time-varying systems that have been employed to investigate various engineering challenges like a metal's electrical impedance changing as a result of pit corrosion [11], varying mechanical loads to bridges and buildings [12], [13], or aeroelastic flutter during flight [14]. In all cases, the system dynamics can be described using a model which is either parametric or nonparametric in its dynamics and time variation. Both parametric and nonparametric models may be used to obtain a time-varying frequency response function (TV-FRF) that provides a description of the time-varying system dynamics. For parametric models, systems are typically described by using differential equations with time-varying coefficients. The differential equations can be expressed in the time or frequency domain to define the assumed model structure [15], [16]. The time-varying coefficients are expressed using time-dependent basis functions, which may be, e.g., wavelets, sines, and cosines, or Legendre

polynomials. Alternatively, time-varying autoregressive moving average (ARMA) models have been successfully applied to estimate TV-FRFs [17].

An example of a nonparametric SI tool to provide a time-dependent spectral representation of a nonstationary signal is the short-time Fourier transform (STFT) [18]. In the STFT, a linear representation of the signals is constructed within a short, fixed-length time window. Subsequently, the TV-FRF is created by sliding the window over time. Other nonparametric tools to analyze nonstationary signals include wavelets and Cohen's class of distributions [18]. These methods have been successfully used to extract time-varying system properties [19], [20]. The advantage of nonparametric models over parametric models is that they require very little to no *a priori* assumptions on the model structure and order [21].

Both parametric and nonparametric models have been used to describe time-varying joint impedance [20]–[29]. A second-order mass-spring-damper system is often assumed to represent joint dynamics. Therefore, a second-order parametric model based on linear differential equations has often been used to describe the joint properties [22]–[24]. For example, a parametric ARMA model has been used to describe elbow stiffness during cyclic movements [25]. Nonparametric models have also been used to describe the joint properties in both the time [4], [26]–[30] and frequency domain [31].

A challenge in estimating time-varying joint properties is the poor signal-to-noise (SNR) ratios of human physiological (-20 dB) and mechanical signals (20–30 dB) [32]. These noise levels are (too) high for accurate identification of joint properties. Therefore, a good model of joint properties can only be obtained by averaging repetitive measurements of the same time-varying behavior before the model is estimated, a process called ensemble averaging. As the noise is typically random the SNR is improved by averaging. When studying the time-varying behaviors, there are various downsides to the need for ensemble averaging. First, it may conceal important adaptations in motor control and interesting trial-to-trial variability [33], [34] of the joint properties and motor performance. Second, as more data are required while the experimental time is limited participants may suffer from muscular fatigue and lapses in attention that will affect the behavior. Therefore, there is an increased need for SI methods that allow for the estimation of joint properties based on a single trial of data, the feasibility of which has been demonstrated previously [17], [35], [36].

The aim of this paper is to validate one parametric and one nonparametric linear time-varying (LTV) SI technique for identifying time-varying joint impedance of the human wrist. This will be done based on single-trial data recorded from a postural task during which participants exert a time-varying flexion torque. The presented methods provide a novel framework for LTV methods to assess time-varying human joint properties with limited experimental constraints.

In Sections II and III, the SI methods employed to study joint impedance are outlined. Section IV describes a simulation study, used to demonstrate the validity of the presented SI methods when identifying known time-varying joint impedance. Following the simulation study, an experimental study was performed which is described in Section V. Finally, in Section VI, the results are interpreted and discussed.

II. Skirt Decomposition Method

In this section, we introduce a nonparametric estimator to identify continuous-time linear time-varying systems. The estimator allows identifying an unknown time-varying system based on the response to a periodic multisine perturbation signal [37].

A. Background

The behavior of a time-varying system G is considered linear with respect to its arbitrary input $u(t)$ and response output $y(t)$. The latter can be computed as

$$y(t) = G\{u(t)\} \equiv \int_{-\infty}^{\infty} g(t,\tau)u(\tau)d\tau \tag{1}$$

where $g(t,\tau)$ is the time-varying impulse response function of G. This means that $g(t,\tau)$ is the response of the system at time t to an impulse applied at time τ. The Fourier transform of the time-varying impulse response function defines the system function or time-varying FRF $G(j\omega,t)$ [38]

$$G(j\omega,t) = \int_{0}^{\infty} g(t,t-\tau)e^{-j\omega\tau}d\tau. \tag{2}$$

The system function $G(j\omega,t)$ relates the Fourier transform of the perturbation signal $U(j\omega)$ to the output signal $y(t)$ as

$$y(t) = \frac{1}{2\pi}\int_{-\infty}^{\infty} G(j\omega,t)U(j\omega)e^{j\omega t}d\omega. \tag{3}$$

For the convenience of the identification procedure elaborated further down, we write the system function $G(j\omega,t)$ as a series expansion

$$G(j\omega,t) = \sum_{p=0}^{\infty} G_p(j\omega)b_p(t) \tag{4}$$

with $\{b_p(t)\}_{p=0}^{\infty}$ representing a complete set of basis functions. These basis function are used to represent the time variation across a series of linear time-invariant (LTI) systems G_p. By inserting (4) into (3), the system behavior is described by

$$y(t) = \sum_{p=0}^{\infty} G_p\{u(t)\}b_p(t) \quad \forall t \in [0,T] \tag{5}$$

where $G_p\{u(t)\}$ is the response of an LTI system G_p to an input $u(t)$ applied during a time window of length T.

B. Identification Procedure

The goal is to extract a nonparametric estimate of the FRFs of the LTI systems $G_p(j\omega)$ for a given (or chosen) set of basis functions. The strategy consists of applying a sparse multisine as excitation signal. The multisine perturbation is defined as

$$u(t) = \sum_{k_e \in K_{exc}} A_{k_e}\cos(\omega_{k_e}t + \phi_{k_e}). \tag{6}$$

Thus, the multisine signal is a sum of cosines, with:

1) angular frequencies $\omega_{k_e} = 2\pi k_e / T_{ms}$, where T_{ms} is the length (in seconds) of the multisine signal;
2) $K_{exc} \subset N$ a sparse set of excited frequency bins, chosen sufficiently separated to ensure the identifiability of the model (as elaborated in [37]);
3) amplitudes A_{k_e}, which, in concordance with K_{exc}, determine the spectral content of the perturbation; and
4) phases ϕ_{k_e}, which are chosen randomly, uniformly distributed in $[0, 2\pi[$.

Considering that a multisine is used as an excitation signal, the system (5) can be rewritten in terms of the discrete Fourier transforms (DFTs) of the perturbation signal, output signal and basis functions [denoted $U(k)$, $Y(k)$, and $B_p(k)$, respectively]

$$Y(k) = \frac{1}{N} \sum_{p=0}^{N_p} \sum_{k_e \in K_{exc}} G_p(j\omega_{k_e}) U(k_e) B_p(k - k_e) + T_Y(j\omega_k) \tag{7}$$

where the sum in (5) has been truncated to the first N_p terms, where N_p is the order of the time variation. $T_Y(j\omega_k)$ captures the transient effects, which are due to the difference between the initial and end conditions of the system. It is assumed that the applied input DFT $U(k)$ is known, and that the measurements $Y_m(k)$ of the output DFT spectrum are available, corrupted by an additive output noise $V(k)$

$$Y_m(k) = Y(k) + V(k). \tag{8}$$

In (7), the output DFT spectrum $Y(k)$ of the system model is linear in the FRFs $G_p(j\omega_{k_e})$, for $p = 0, \ldots, N_p$ and $k_e \in K_{exc}$. Thus, these FRFs can be extracted from the measured output by a linear least squares algorithm. This results in a maximum likelihood estimator under some weak assumptions (Assumption 7 in [37]) on the measurement noise $V(k)$ (which should be uncorrelated over the frequencies) and for an implementation in a sliding frequency domain window, as explained in Appendix A. Note that G_p is only estimated at a discrete set of frequencies (known as the excited frequencies of the multisine). For this reason, this estimate is called "nonparametric."

The sparsity of the multisine is important to obtain a well-posed problem. Namely, in (7), the number of unknowns equals $N_p \cdot N_{exc}$ (where N_{exc} is the cardinality of K_{exc}, i.e., the number of excited frequencies). A necessary condition for the problem to have a unique solution is that $N_p \cdot N_{exc}$ is smaller than the number of data points (which equals the number of bins in the frequency band of interest). This is illustrated in Fig. 1, for $N_p = 7$. The black dots give the output spectrum $Y(k)$ in a limited frequency band, which comprises three excited frequencies (vertical arrows). Due to the time-varying character of the system, the output spectrum consists of skirt-shaped contributions around the excited frequencies. These "skirts" are modeled in (7) as linear combinations of terms of the form $G_p(j\omega_{k_e}) U(k_e) B_p(k - k_e)$. Hence, the sparsity of the set of excited frequencies is important to enable distinguishing the individual terms.

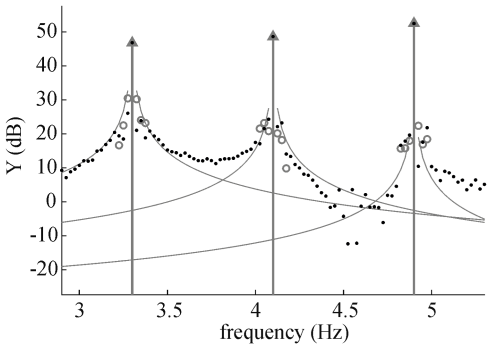

Fig. 1. The black dots give the output spectrum of a time-varying system, excited by a sparse multisine. This output spectrum is decomposed into: 1) excited frequencies (vertical arrows); 2) skirt shaped contributions (gray full lines); and 3) discrete spectral contributions (gray circles) which are due to the periodic nature of the applied time variation.

III. Kernel-Based Regression Method

In this section, we introduce a parametric estimator to identify the continuous-time linear time-varying systems. The estimator is adopted as suggested in [39].

The system's input and output signals, $u(t)$ and $y(t)$, are assumed to satisfy a linear differential equation of the form

$$y(t) = -\sum_{n=1}^{N_a} a_n(t) \frac{d^n y(t)}{dt^n} + \sum_{n=0}^{N_b} b_n(t) \frac{d^n u(t)}{dt^n} \tag{9}$$

where $a_n(t)$ and $b_n(t)$ are the time-varying coefficients which are smooth functions of t. These coefficients are estimated via kernel-based regression (KBR). In essence, the estimator is defined as the following minimizer:

$$\hat{a}_n, \hat{b}_n = \underset{a_n, b_n}{\operatorname{argmin}} \sum_{k \in K_{int}} \frac{|E(k, a_n, b_n)|^2}{\hat{\sigma}_E^2(k, a_n, b_n)} + R(a_n, b_n) \tag{10}$$

where E is the DFT of the equation error [i.e., the difference between the left- and right-hand sides of (9)], evaluated in K_{int}, and a_n and b_n are vectorised versions of $a_n(t)$ and $b_n(t)$ in $t = 0, T_s, \ldots, (N-1)T_s$. K_{int} represents the bins of the frequency band of interest and $\hat{\sigma}_E^2$ is (an estimate of) the noise variance of E. $R(a_n, b_n)$ is a quadratic regularization term, to impose the smoothness of the estimates. This is elaborated in more detail in Appendix B, and in Lataire *et al.* [39].

IV. Simulation Study

In this section, a simulation study is described to confirm the validity of the SI methods with a known time-varying stiffness.

A. Modeling Human Joint Dynamics

A time-varying wrist stiffness is simulated using a model describing endpoint dynamics of a joint interacting with an 1-DOF robotic manipulator. The dynamics of the joint, when only small rotations are applied, can be represented by a simple second-order IBK model $H_i(s)$ together with the viscoelasticity of the interaction between manipulator

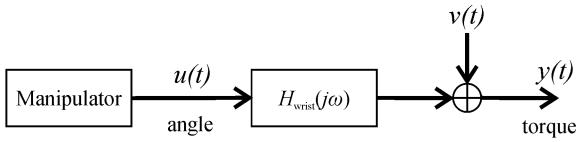

Fig. 2. System of the human wrist. The manipulator provides a multisine position input $\boldsymbol{u(t)}$ to the human wrist of which the dynamics are represented by $\boldsymbol{H_{wrist}(j\omega)}$. The measured torque output $\boldsymbol{y(t)}$ is assumed to contain measurement noise $\boldsymbol{v(t)}$.

and human $H_c(s)$ [1]

$$H_i(s) = \frac{1}{Is^2 + bs + k} \tag{11}$$

$$H_c(s) = b_c s + k_c \tag{12}$$

in which s is the Laplace variable and equals $j2\pi f$ (f represents the frequency) when evaluated on the imaginary axis. $H_i(s)$ represents the intrinsic and reflexive joint dynamics where I is the limb inertia, b is the joint viscosity, and k is the static joint stiffness. $H_c(s)$ represents the contact dynamics, a simple spring-damper system where b_c is the contact viscosity and k_c is the contact stiffness.

The overall system representing the mechanical joint impedance from joint angle [$u(t)$-and taken equivalent to the angle of the handle of the manipulator] to joint torque [$y(t)$] is then

$$\begin{aligned} H_{\text{wrist}}(s) &= \frac{H_c(s)}{1 + H_c(s)H_i(s)} \\ &= \frac{Is^3 + (b_c b + k_c I)s^2 + (b_c k + k_c b)s + kk_c}{Is^2 + (b + b_c)s + (k + k_c)} \end{aligned} \tag{13}$$

The system considered is shown in Fig. 2.

B. Model Implementation

The system as presented in Fig. 2 was implemented in MATLAB 2017b-Simulink 9.0 (The MathWorks, Inc., Natick, MA, USA). Output noise $v(t)$ was added as a 15-Hz low-pass filtered (second-order Butterworth) Gaussian white noise. The amplitude of the noise was scaled such to result in the desired SNR.

C. Simulation Parameters

The system, representing a human wrist joint, was simulated for 50 s ($f_s = 2500$ Hz), with a time-varying joint stiffness (k) between ~4.7 and 6.5 Nm/rad. Limb inertia (I) and joint viscosity (b) were considered time-invariant and taken as 3 gm^2 and 0.035 Nms/rad, respectively. Contact dynamics was also considered time invariant ($b_c = 10$ Nms/rad, $k_c = 100$ Nm/rad).

First, to demonstrate the attributes of the used algorithms, a time-varying joint stiffness using a square wave with a period of 10, 20, and 30 s was simulated at three noise levels (SNR: Inf, 10 or 5 dB). A square wave allows revealing how well the instantaneous changes in joint dynamics can be followed by the algorithms. For each noise condition, two trials were simulated with the same input signal but different noise realization: one to perform an estimation of joint dynamics and the other for validation.

Second, joint stiffness was varied sinusoidally with a period of 20 s (0.05 Hz) and two trials were simulated, one for estimation and one for validation, for each of the three studied noise levels.

D. Perturbation Signal Design

Random-phase multisine perturbations were used as the input signal to the simulations. Each multisine perturbation signal had a period of 10 s with excited frequencies 0.1–19.3 Hz and a spacing of 0.8 Hz between the excited frequencies. The perturbation signal was designed such that the rotation of the wrist had a root-mean-square (rms) value of ≈1.1° (0.02 rad). A perturbation signal with a bandwidth limited to 20 Hz is able to reveal all relevant wrist joint dynamics [40]. The magnitude of each excited frequency was constant up to 6 Hz and decreased at higher frequencies (slope of −20 dB/decade).

E. Data Analysis

Before applying the KBR and the skirt decomposition identification algorithms, the data were decimated in the frequency domain to a sampling frequency of ~44 Hz. Subsequently, the data of the first and last 5 s of each trial was discarded as it was only used for initialization and did not contain a perturbation. Finally, data are only shown in the time interval [0, 30] s. The estimate in the intervals [−5, 0] s and [30, 35] s is unreliable because of initial transient effects.

Skirt Decomposition: For the skirt decomposition method, the basis functions $b_p(t)$ used in this paper are the following:

$$\begin{aligned} b_0(t) &= 1 \\ \mathrm{b_1(t)} &= \mathrm{2t/T - 1} \\ b_p(t) &= \cos(\omega_{p/2}t), \quad p > 1, \ p\text{even} \\ b_p(t) &= \sin(\omega_{(p-1)/2}t), \quad p > 1, \ p \text{ odd}. \end{aligned} \tag{14}$$

Considering $B_p(k) = \mathrm{DFT}\{b_p(t)\}$, the individual terms $G_p(j\omega_{k_e})U(k_e)B_p(k - k_e)$ from (7) can be recognized in Fig. 1:

1) The vertical arrows (excited frequencies) are terms with $p = 0$. Since b_0 is a constant, see (14), $B_0(k - k_e)$ is only different from 0 when $k = k_e$ in (7).
2) The gray full lines are terms with $p = 1$. With b_1 being a ramp, $B_1(k - k_e)$ is an (approximate) hyperbolic function, centered around the excited frequency bin k_e.
3) The gray circles are terms for $p > 1$. (Co)sines have discrete Fourier transforms, which allow to capture individual bins of the output spectrum, at both sides of each excited frequency.

Since b_0 is a constant, and $b_p(t)$ for $p > 0$ is zero mean in the measured time window (T), G_0 represents the best LTI approximation of the system, as defined in [41] and [42]. (Co)sines are included as basis functions in (14) to account for the periodic nature of the imposed time variation.

The order of the time variation was set to $N_p = 7$. This is motivated by the observation that, in about six unexcited bins around the excited frequency (namely three to its left and three to its right), the output spectrum has a value which is significantly higher than the noise. By using $N_p = 7$, we have a total of six goniometric basis functions (14), which allow to capture these six bins.

Kernel-Based Regression: In this paper, for the KBR method, outlined in Section III, the regularization term R uses a kernel matrix K obtained from the squared exponential kernel

$$K(t, t') = \gamma\, e^{\frac{-(t-t')^2}{\sigma^2}}, \quad t, t' = 0,\ T_s, \ldots, (N-1)T_s \tag{15}$$

in which σ determines the smoothness of the estimated time-varying coefficients. The hyperparameter γ represents the inverse of the amount of regularization applied, defining a bias versus variance tradeoff of the estimated coefficients. The hyperparameters γ and σ together determine the complexity of the estimated model.

The assumed model structure has a third-order numerator and second-order denominator, based on the assumed system of joint impedance (13). Therefore, the parameter N_a was chosen as 2 and N_b as 3. We define the frozen transfer function of the time-varying system as

$$H_{\text{wrist}}(s, t^*) = \frac{b_3(t^*)s^3 + b_2(t^*)s^2 + b_1(t^*)s + b_0(t^*)}{a_2(t^*)s^2 + a_1(t^*)s + a_0(t^*)} \tag{16}$$

When evaluated in t^*, the function $H_{\text{wrist}}(s, t^*)$ is the transfer function of the LTI system, obtained by fixing the time-varying parameters to their values at time instant t^*, i.e., $a_n(t^*)$ and $b_n(t^*)$.

The hyperparameter σ was chosen based on the periodicity of the time-varying stiffness as $\sigma \approx 20\ s$ in case of the presence of noise. This is to comply with the experimental study and demonstrate how σ affects the estimates with different noise levels and speed of the dynamics. For the noiseless case, σ was reduced to $\sim$8 s. This increases the flexibility of the estimator and, thus, reduces the bias (this is important to show the correctness of the estimator). In addition, γ was chosen based on the variance of the data in presence of noise as the estimate was insensitive to the precise value of γ in a wide range. When no noise was present in the simulation, γ was set to 25.000.

Quality of the Estimators: The quality of the estimators was determined in the time domain using the variance-accounted-for (VAF). The VAF was calculated according to

$$\text{VAF} = 1 - \frac{\text{var}(y(t) - \hat{y}(t))}{\text{var}(y(t))} \tag{17}$$

where $y(t)$ is the simulated torque and $\hat{y}(t)$ is the estimated output torque based on the identified model of joint impedance. Three VAF values were calculated:

1) VAF_{self}: where $\hat{y}(t)$ is calculated and compared to $y(t)$ that was used to estimate the joint impedance model (including output noise).
2) $\text{VAF}_{\text{optim}}$: where $\hat{y}(t)$ is calculated and compared to a simulated output torque $y(t)$ without output noise-representing the highest achievable VAF when using noisy data to estimate the joint impedance model.
3) VAF_{val}: where $\hat{y}(t)$ is calculated and compared to a simulated output torque $y(t)$ with output noise but a different noise realization (the second "validation" trial simulated).

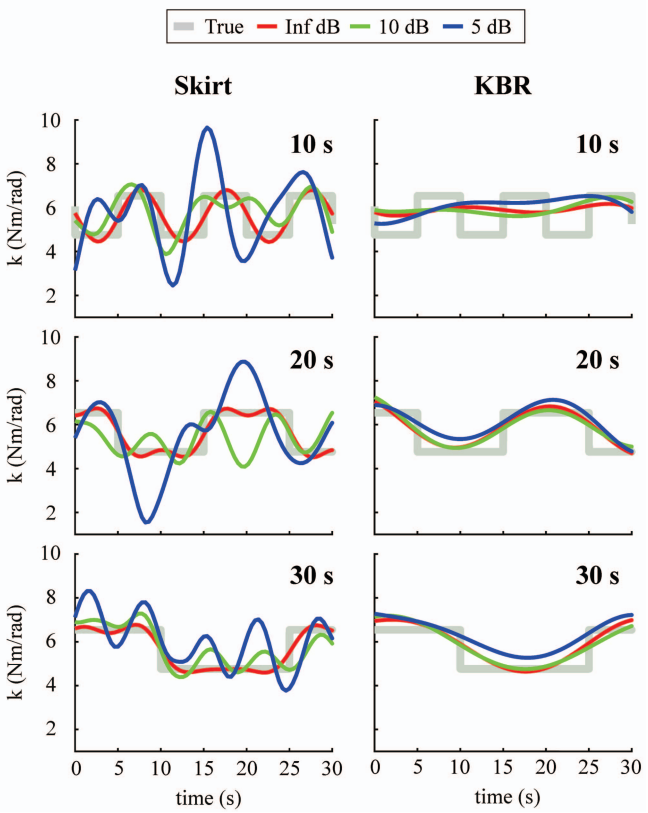

Fig. 3. Joint stiffness estimates obtained using the KBR and skirt method from simulation data. Simulations were run including a time-varying joint stiffness following a square wave with different periods (10, 20, and 30 s) both without (SNR = Inf dB) and with (SNR = 5 or 10 dB) output noise. The skirt decomposition method can estimate the sharp transitions in stiffness for the square waves with longer periodicity but the estimates are sensitive to noise. The estimates of joint stiffness using the KBR are less sensitive to noise but are smooth, i.e., cannot estimate rapid transitions in joint stiffness, because of the adopted values for the hyperparameters.

In addition, the true simulated joint stiffness and estimated joint stiffness, extracted as the magnitude of the FRF at the lowest frequency, were compared. The root-mean-square error (RMSE) between simulated (k_i) and estimated ($\hat{k}_i$) joint stiffness was calculated using the following equation:

$$\text{RMSE}_k = \sqrt{\frac{\sum_{i=1}^{N} (k_i - \hat{k}_i)^2}{N}} \tag{18}$$

where the difference in simulated and estimated joint stiffness is summed for all time points i in the time series of length N. For this paper, the difference between system function or TV-FRF (2) and frozen FRF as extracted from (9), are neglected.

F. Results

Figs. 3 and 4 present the estimated joint stiffness as a function of time in comparison to the known true stiffness as

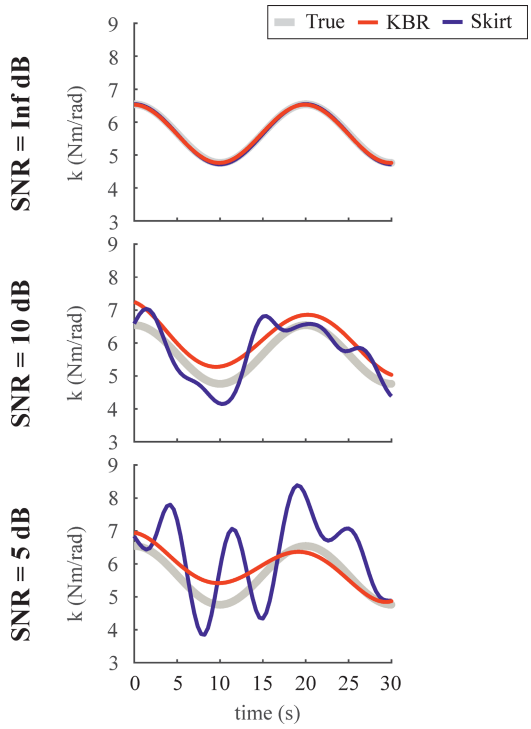

Fig. 4. Joint stiffness estimates obtained using the KBR and skirt method from simulation data. Simulations were run including a time-varying joint stiffness both without (SNR = Inf dB) and with (SNR = 5 or 10 dB) output noise. Both the KBR and skirt method allow obtaining a good estimate of joint stiffness despite the presence of 10 dB output noise, but the skirt decomposition method performs not so well with 5 dB noise.

imposed in the simulation. When the joint stiffness is varied using a square wave, the skirt method is able to estimate joint stiffness well in case the variation is slow (20 or 30 s) and noise levels are low (>10 dB). The KBR method also performs better for slower time-varying conditions, but is unable to track the step transitions in stiffness. This is reflected in Table I, presenting VAF and RMSE_k. Hence, whereas VAF_val is higher and RMSE_k lower for the KBR method in presence of noise, the skirt method better estimates the time-varying joint stiffness when no noise is present (smaller RMSE_k).

For the sinusoidally time-varying joint stiffness (Fig. 4), the true and estimated stiffness closely match for both analysis methods when there is no noise. Identification of the joint stiffness from a simulation trial with an SNR of 10 dB still allows extracting the sinusoidal periodicity, but with a mismatch to the true stiffness. The estimate of joint stiffness by the skirt method is more affected by the presence of noise than the KBR method (lower VAF_val and RMSE_k). Table I shows that based on the VAF on the estimation data (with noise) both methods provide a good model for the data ($\text{VAF}_\text{self} > 96\%$). When validating the model, VAF is still high ($\text{VAF}_\text{val} > 94\%$). The KBR method achieves a higher VAF ($\text{VAF}_\text{val} = 96.7\%$) on the validation set then the skirt method ($\text{VAF}_\text{val} = 94.9\%$). Both methods provide an excellent estimate of the true FRF despite the noise as evident from the VAF on a trial without noise ($\text{VAF}_\text{optim} > 98\%$). The KBR method ($\text{VAF}_\text{optim} = 99.9\%$) outperforms the skirt method ($\text{VAF}_\text{optim} = 98.2\%$).

V. Experimental Study

This section describes how the experimental study was performed.

A. Subjects

Six healthy participants (two men, 33 ± 4.2 years; four women, 28 ± 4.1 years) with no self-reported history of neurological or orthopedic arm problems, participated in the experiment. All participants were right handed. The study was approved by the human research ethics committee of Delft University of Technology, and all participants provided written informed consent before participating.

B. Experimental Setup

A torque-controlled wrist manipulator applied angular position perturbations to the wrist of the right arm [43]. The manipulators' handle is actuated by an electric motor (Baumuller DSM-130N) via a lever which ensures the motor axis is aligned with the axis of rotation of an average wrist. A torque sensor, consisting of strain gages, was mounted halfway the lever to measure the torque applied by the participant. The core of the haptic controller is its velocity servo, which has a bandwidth of ~50 Hz.

Every participant was comfortably seated in front of the manipulator and asked to grab the handle with the right hand. To ensure a firm and time-invariant grip, Velcro was used to strap participants to the handle and the lower arm was immobilized. During the perturbations, the participants were asked to apply a prescribed time-varying torque. A screen in direct line of sight of the participant provided a target line, representing the torque that had to be exerted, and a cursor that was indicative for the exerted torque (0.6-Hz low-pass filtered). Participants were instructed to trace the target line with the cursor throughout each trial. Fig. 5 provides a schematic of the experimental setup. During all trials, the torque on the handle and position of the handle were measured, sampled at 2500 Hz and stored.

C. Measurement Protocol

The participants completed 12 trials, six trials each for two different tasks. Before the trials, the maximum voluntary torque (MVT) was determined. The first task required the voluntary modulation of flexion torque. Participants had to vary their exerted flexion torque between 5% and 20% MVT according to a sinusoidal pattern (with a period of 20 s, frequency of 0.05 Hz). Participants were instructed to track a target line presented on the screen while ignoring the continuous multisine angular perturbation on the handle of the manipulator. The torque variations due to the perturbation were much smaller than the requested voluntary modulation. Each trial lasted 50 s, including 5 s at the start and end of each trial without perturbation. The second task was a time-invariant condition, without bias force, where participants were instructed to keep their wrist relaxed while angular perturbations were applied. For both tasks, the same perturbation signal was used as during the simulation study with the rotation of

TABLE I
VAFs AND $RMSE_k$ FOR SIMULATION DATA

		Noise [dB]	VAF_{self} [%]	VAF_{optim} [%]	VAF_{val} [%]	$RMSE_k$ [Nm/rad]
Sine	**KBR**	5	89.9	99.7	89.7	0.42
		10	96.7	99.9	96.7	0.46
		Inf	99.9	-	-	0.02
	Skirt	5	92.4	94.7	84.4	1.24
		10	97.7	98.2	94.9	0.9
		Inf	99.9	-	-	0.03
Square 10 s	**KBR**	5	89.4	98.9	89.4	0.95
		10	96.3	99.2	96	0.86
		Inf	99.3	-	-	0.84
	Skirt	5	93.3	93.7	84.1	2.02
		10	97.3	97.7	94.6	1.17
		Inf	99.9	-	-	0.39
Square 20 s	**KBR**	5	90.3	99.4	89.8	0.63
		10	96.3	99.2	96.0	0.56
		Inf	99.8	-	-	0.47
	Skirt	5	92.5	93.6	84.2	1.55
		10	97.7	98.1	94.9	1.22
		Inf	99.9	-	-	0.27
Square 30 s	**KBR**	5	90.1	99.5	89.7	0.75
		10	96.6	99.8	96.5	0.45
		Inf	99.9	-	-	0.42
	Skirt	5	93.4	94.3	84.1	1.34
		10	97.6	97.9	94.6	0.93
		Inf	99.9	-	-	0.25

Variance-Accounted-For (VAF) and root mean square error of the estimated compared to the known present stiffness ($RMSE_k$), for both KBR and skirt method when using simulation data with and without noise. The model estimate is based on a single trial with 5 dB, 10 dB or no (Inf dB) filtered white noise and validated on de data used for estimation (VAF_{self}). In addition, validation is performed on a trial without noise (VAF_{optim}) and trial with different noise realization but same noise level (VAF_{val}).

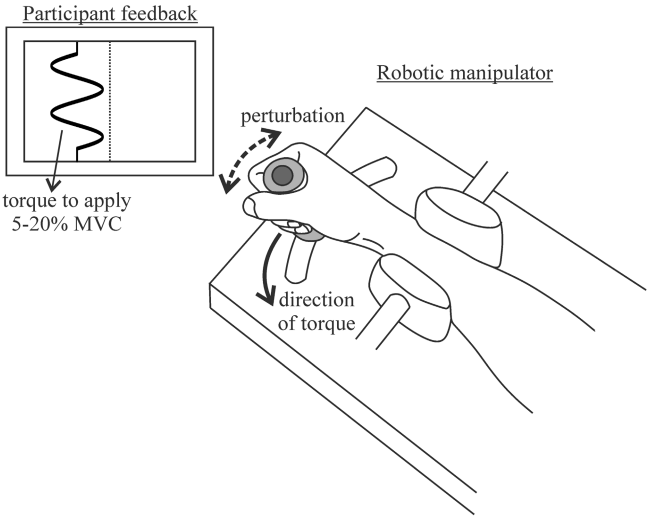

Fig. 5. Experimental setup used to measure time-varying joint impedance. The right arm of the participant was fixated, with the flexion-extension axis of the wrist aligned with the axis of rotation of the handle of the manipulator. Multisine position perturbations were imposed on the handle while the participant had to track a sinusoidal torque pattern. Feedback on torque exerted and target torque level was provided on a monitor directly in front of the participant.

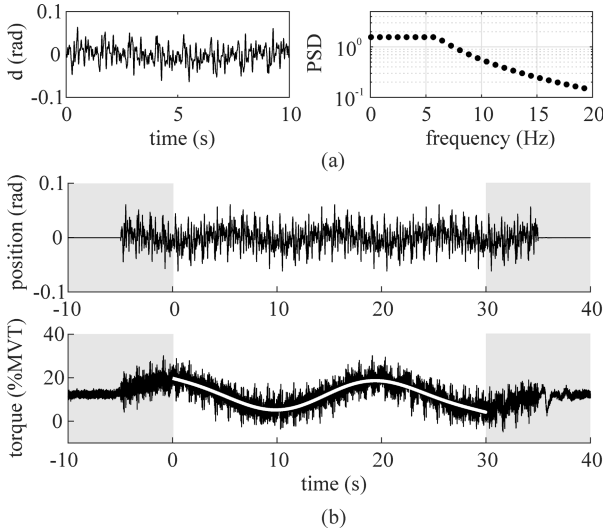

Fig. 6. Details of perturbation signal and raw data recorded. (a) Position perturbation signal in frequency and time domain. Perturbation signal is built of 10 s periods, containing only frequencies between 0.1 and 19.3 Hz ($\Delta f = 0.8$ Hz). (b) Raw position and torque data recorded during a single trial. The shaded areas are data not analyzed to avoid modeling artifacts or transient effects. The voluntary exerted sinusoidal time-varying torque (white line) was removed prior to analysis, as it only served to obtain time-varying joint impedance.

the wrist restricted to 0.02 rad and excited frequencies between 0.1 and 19.3 Hz (Section IV-D and Fig. 6(a)).

D. Data Analysis

The same data preprocessing was performed as for the simulation study: part of the data were discarded and the remaining data were decimated.

The exerted time-varying voluntary torque was applied to ensure time-varying joint properties, but is not relevant for the estimator. Therefore, before performing SI, the 0.05 Hz time-varying voluntary exerted torque was removed by fitting and subtracting a low-frequency signal composed of a

constant, a linear function and four goniometric functions [cos (ωt), sin (ωt), cos ($2\omega t$), sin ($2\omega t$)], where ω is the lowest frequency fitting the analyzed time window (T), i.e., $1/T$, and in this paper, $1/40 = 0.025$ Hz [Fig. 6(b)—white solid line].

For the skirt decomposition and KBR method, the same model structure and parameters were used as during the simulation study. The order of the time variation for the skirt method was set to $N_p = 7$ and the hyperparameter σ for the KBR method was set to ~20 s, with γ based on the variance of the data.

Quality of the Estimators: The quality of the estimators was assessed using the VAF (17). VAF was determined twice:

1) VAF_{self}: where the estimated torque $\hat{y}(t)$ is calculated and compared to the measured output torque $y(t)$ that was used to estimate the joint impedance model.
2) VAF_{val}: where the estimated torque $\hat{y}(t)$ is calculated and compared to the measured output torque $y(t)$ of the five trials not used for estimation of the joint impedance model.

Before determining the VAF, frequencies below 0.8 Hz were removed as these frequencies are dominated by trial-to-trial variability in voluntary motor control and have little contribution to joint dynamics.

E. Comparison With Other Techniques

The two proposed identification methods for joint impedance were compared with two other methods previously presented. Both methods are ensemble averaging methods, requiring multiple repetitions of the same time-varying behavior. The first is a method proposed by Ludvig and Perreault [44] who used a nonparametric estimator in the time domain to successfully identify joint impedance averaging across short data segments (SDS) and multiple (but a reduced number of) realizations [27]. We implemented this method ourselves. The second method is one designed by Guarin and Kearney [45] (scripts available online) who combine ensemble and deterministic approaches to estimate TV joint impedance.

For a fair comparison of the methods, those presented in this paper and those by Guarin and Ludvig, five of the six collected trials are used as an input for estimating the joint impedance model and the sixth trial is used for validation. Before analysis, data were decimated to 100 Hz to limit the computational burden. For the SDS method, we used a window length of 100 samples (1 s), i.e., this is the time window over which the joint impedance is considered time-invariant, and a maximum lag of the impulse response function of 40 ms.

F. Results

Position and torque data are presented in Fig. 6(b). The position data are equivalent to the imposed perturbation. Torque data show the torque exerted by the participant, expressed as a percentage of their maximum voluntary torque level, on top of the rapid torque changes as resulting from the applied position perturbation.

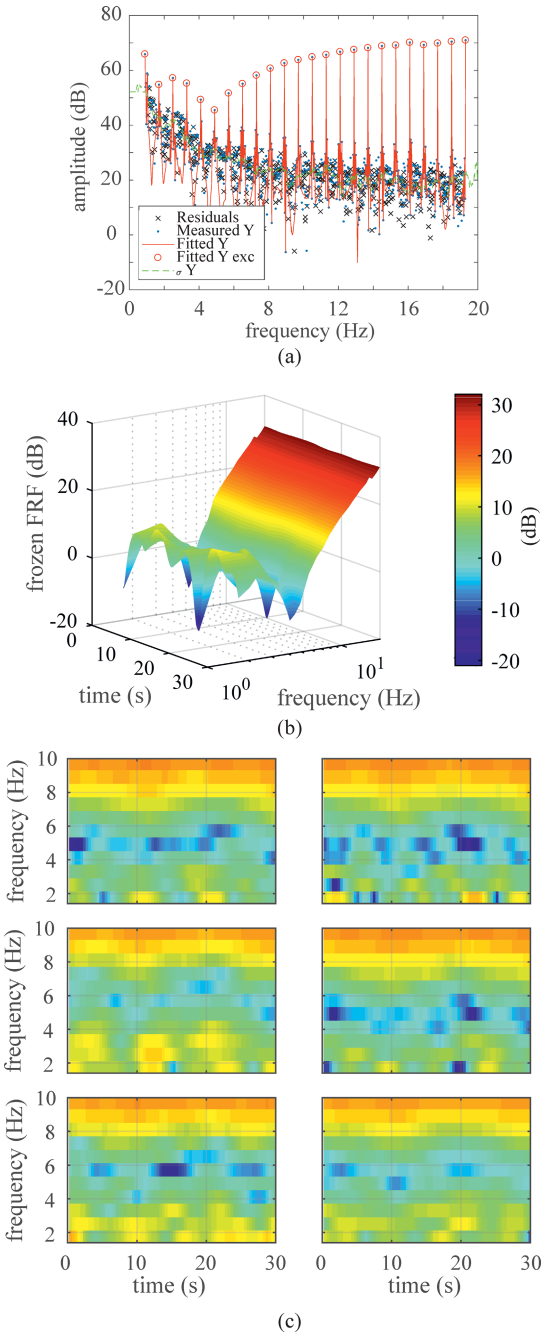

Fig. 7. Results obtained using the skirt decomposition method. (a) Measured (dots) output spectrum, fitted (red line) output spectrum and their difference (residuals – crosses). The green line indicates the noise floor. (b) Estimated system function, as defined in (2) with the estimated $\mathbf{G_p}$. (c) System function for all trials recorded for a single participant in the condition where voluntary torque was sinusoidally varied between 5% and 20% of maximum voluntary torque. Color scale same as in (b).

Skirt Decomposition Method

Fig. 7 presents the results obtained when using the skirt decomposition method on the experimental data. The measured and fitted output spectrum were well matched at, and close to, the excited frequencies [Fig. 7(a)]. The green dashed line gives the estimated noise floor.

The corresponding system function shows a sinusoidally varying joint stiffness and resonance frequency analog to the sinusoidal exerted voluntary torque [Fig. 7(b)]. This is

TABLE II
VAFs FOR EXPERIMENTAL DATA

	Single trial				Ensemble			
	KBR		Skirt		KBR	Skirt	SDS	Guarin
	VAF_{self} [%] mean±S.D.	VAF_{val} [%] mean±S.D	VAF_{self} [%] mean±S.D	VAF_{val} [%] mean±S.D	VAF_{val} [%] mean±S.D	VAF_{val} [%] mean±S.D	VAF_{val} [%] mean±S.D	VAF_{val} [%] mean±S.D
P1	89.7 ± 3.0	89.1 ± 2.9	91.2 ± 3.3	82.9 ± 3.3	89.2 ± 2.9	87.3 ± 3.2	88.0 ± 2.7	88.0 ± 2.9
P2	88.8 ± 5.0	88.1 ± 4.5	90.8 ± 3.9	81.8 ± 3.9	88.6 ± 4.8	86.5 ± 3.8	88.3 ± 5.2	88.0 ± 4.5
P3	80.8 ± 8.7	79.9 ± 9.0	85.5 ± 7.3	76.2 ± 6.9	80.6 ± 8.6	80.0 ± 5.1	80.3 ± 9.3	80.0 ± 8.6
P4	52.4 ± 14.5	51.4 ± 14.2	66.1 ± 8.0	39.8 ± 9.3	52.4 ± 14.5	51.8 ± 9.4	51.6 ± 13.8	48.9 ± 14.9
P5	75.8 ± 5.2	75.4 ± 5.5	86.3 ± 3.1	66.7 ± 7.2	75.8 ± 5.2	74.7 ± 7.3	75.1 ± 5.5	74.0 ± 5.3
P6	70.9 ± 7.4	71.3 ± 7.4	85.8 ± 2.2	60.6 ± 4.8	71.1 ± 7.5	71.6 ± 3.5	69.8 ± 6.7	68.7 ± 7.2
Overall	**76.4 ± 7.3**	**75.8 ± 7.3**	**84.3 ± 4.6**	**66.1 ± 6.0**	**76.3 ± 7.2**	**75.3 ± 5.4**	**75.5 ± 7.2**	**74.6 ± 7.2**

Variance-Accounted-For (VAF) for both KBR and skirt method when using experimental data. The left side shows VAFs for each participant when estimates were based on a single trial of data. Mean ± S.D. of 6 VAFs is shown when validation is performed on the data used for estimation (VAF_{self}), and 30 VAFs when the one trial is used for estimation and the other five for validation (VAF_{val}),. The right side of the table shows VAFs for four different methods (KBR, Skirt decomposition, Short Data Segments (SDS) and Guarin) when the ensemble average of 5 trials was used for model estimation and the sixth trial for validation (e.g. Mean ± S.D. of 36 VAFs).

highlighted in its 2-D representation [Fig. 7(c)–top left]. Fig. 7(c) shows the system function of all six trials recorded for this participant. All trials demonstrate a sinusoidal-like change in joint stiffness and resonance frequency, however with marked inter-trial variability. Altogether, VAF_{self} for the nonparametric skirt decomposition method for all trials and all participants was on average 84.3% ± 4.6% [(mean ± standard deviation (SD)] (range for individual participants: 66%–91%) (Table II). The estimated model for joint impedance estimated on a single trial was validated on the other five trials. On average, this resulted in a VAF_{val} of 66.1% ± 6.0% (mean ± SD) (range for individual participants: 40%–83%).

Analysis of the task without bias force, i.e., no time-varying behavior, confirmed the time-invariant joint dynamics with a similar resonance frequency across the full-time window. Moreover, VAF_{self} and VAF_{val} were >93% for all trials of all participants.

KBR Identification

Fig. 8 presents the results obtained when using KBR identification with the recorded data. The frozen FRF [Fig. 8(a)] demonstrates a sinusoidally varying joint stiffness and resonance frequency, for all trials performed by this participant [Fig. 8(b)]. The VAF_{self} for the parametric KBR identification method on the trials performed by the first participant was on average 76.4% ± 7.3% (mean ± SD) (range for individual participants: 52%–90%) (Table II). The estimated model for joint impedance estimated on a single trial was validated on the other five trials. On average, this resulted in a VAF_{val} of 75.8% ± 7.3% (mean ± SD) (range for individual participants: 51%–89%).

Analysis of the task without bias force, i.e., no time-varying behavior, confirmed time-invariant joint dynamics with a similar resonance frequency across the full-time window. Moreover, VAF_{self} and VAF_{val} were >97% for all trials of all participants.

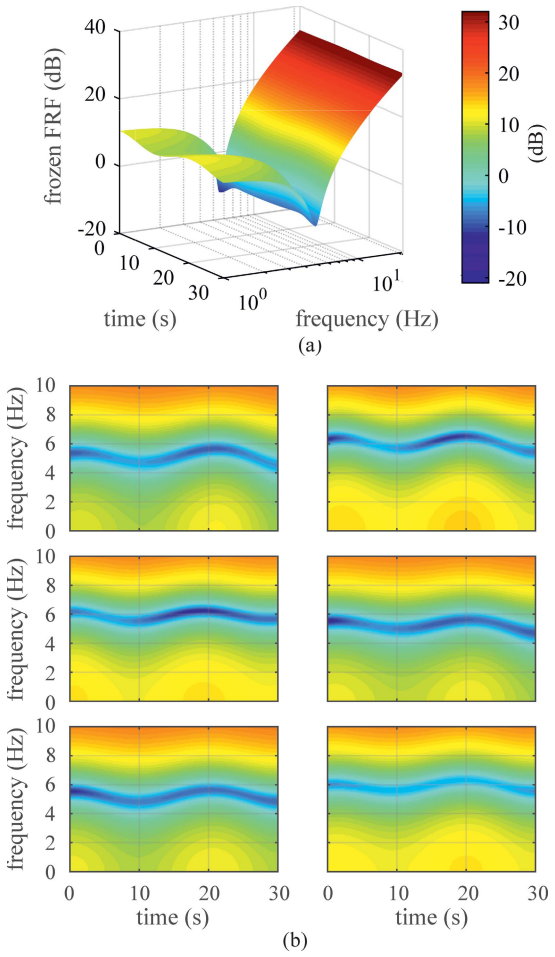

Fig. 8. Results obtained using the kernel-based method. (a) Estimated frozen FRF, using kernel-based regression. (b) Frozen FRF for all trials recorded in a single participant in the condition where voluntary torque was sinusoidally varied between 5% and 20% of maximum voluntary torque. Color scale same as in (a).

Comparison With Other Techniques

Table II presents the VAF for all participants when ensemble data was used in five trials for estimating the joint impedance model, and the sixth trial was used for validation. In addition to the KBR and skirt method, the results are presented for the SDS and Guarin method. On average, the KBR method provides the best results (VAF_{val} = 76.8%±7.2%) closely followed by the SDS, skirt and Guarin method (SDS: VAF_{val} =

75.5% ± 7.2%; skirt: VAF_{val} = 75.3% ± 5.4%; Guarin: VAF_{val} = 74.6% ± 7.2%).

VI. Discussion

In this section, results from the simulation and experimental study will be discussed in light of the new identification procedures to quantify joint impedance.

A. Parametric and Nonparametric Identification of Joint Impedance

This paper demonstrates that it is possible to obtain a good model fit based on a single trial of data, in line with some other recent studies [35], [36]. Both the KBR method and skirt decomposition method revealed a sinusoidal time-varying resonance frequency and joint stiffness. The time-varying system dynamics of the human wrist resembled the time-varying simulated joint stiffness or instructed joint torque. Both algorithms require little *a priori* information about the expected time variations. The minimal information provided to the estimator about time-varying behavior contrasts the commonly employed linear parameter varying (LPV) models. LPV models require a measured time-dependent scheduling function that induces the change of the model parameters [35], [46]. There are no assumptions about the order of the system dynamics, or a scheduling variable, in the skirt decomposition method, but it assumes that the time variations can be described by a set of smooth basis functions. For the KBR method, the order of the system dynamics is set *a priori* and the hyperparameter σ determines the smoothness of the time variation.

The performance of the KBR method depends on the choice of the model order and on the values for the hyperparameters σ and γ. Although a second-order joint impedance model has been used often in the literature, in this paper, a third-order model (three zeros, two poles) was used. The choice for a third-order model structure was based on the joint dynamics (modeled as a second-order mass-spring-damper system) and the grip dynamics to capture the interaction between the joint and the manipulator [1]. A third-order model may better capture the musculoskeletal structure for joints where multiple muscles act around (a joint agonist-antagonist muscle pairs) [47]. Fixed values were used for the hyperparameters in the presence of noise. Lataire *et al.* [39] developed an optimization procedure to determine the optimal values for the hyperparameters by minimizing a leave-two-out-cross validation criterion (LTO-CV) [48]. However, this criterion proved to be fairly insensitive to the value of the hyperparameters, as soon as they are in an acceptable range. Hyperparameter σ was chosen in accordance with our expectations; $\sigma \approx 20$s, which is of the same order of magnitude as the period of the exerted time variation. This value ensures that the resulting estimate is smooth, effectively suppressing noise contributions. The hyperparameter γ was chosen near the global minima of the LTO-CV evaluated for all the trials, as our results were insensitive to the exact value of γ.

The nonparametric skirt decomposition method does not require an *a priori* defined model order and thereby has more flexibility to capture the dynamics, albeit smooth, as dictated by the basis functions used. The method needs a multisine perturbation signal that includes sufficient excited frequencies to quantify the system dynamics and at the same time leaves appropriate space between excited frequencies to capture the time variations in the skirts. When measuring humans, the frequency resolution is limited as the measurement time in humans is restricted, e.g., to prevent fatigue. This is critical at the lowest frequencies up to ∼5 Hz, where the human has the ability to modulate his/her joint impedance. Hence, up to 5 Hz, ideally, there are many excited frequencies that allow proper identification of joint impedance but at the same time, sufficient unexcited frequencies are required to capture time-varying behavior. The nonparametric nature of the skirt method provides more freedom at the cost of a greater variance, especially below the resonance frequency.

For both methods, a well-defined LTV model could be constructed using only a single trial of 30 s of data (VAF_{val} > 70%). Up to ∼90% of the data could be explained using either the KBR method or the skirt based method (on the estimation data set). An explanation for the high VAFs (>85%) in some and low VAFs (<70%) in others may be found in the sensitivity of the methods to the smoothness of the time variation, i.e., data sets from participants that were better at smoothly following a sinusoidally time-varying torque resulted in higher VAFs. The skirt method suffers less from this as no *a priori* model structure is applied. However, the lower VAFs on validation data compared to estimation data (drop by ∼10%–20%), not seen for the KBR method, may indicate overfitting. It is noteworthy that validation based on single-trial data may not only reflect modeling errors but will also be negatively affected due to inherent human trial-to-trial variability. This is reflected in the results of the trials without bias force, i.e., participants are fully relaxed, which result in a higher VAF as the human does not intervene. Moreover, the trials without bias force demonstrate that the methods do not have any *a priori* assumptions on time variance since they fit time-invariant data well.

In the present paper, the comparison with ensemble-based methods of Ludvig and Perreault [4] (SDS) and Guarin and Kearney [45] (Guarin) revealed minimal differences. However, both the SDS and Guarin method were developed with a pseudorandom perturbation signal and for identification of fast time-varying behavior (0.5 Hz), which is different from a multisine perturbation and slow time-varying behavior (0.05 Hz) as applied in this paper. Therefore, the only conclusion to draw from the comparison is that each algorithm can perform well, but that the choice for a specific time-varying system identification technique is driven by the research aim and experimental possibilities.

B. Limitations of the Methods

A potential limitation of the methods is the speed of time variation that can be successfully identified. The 0.05-Hz time-varying torque that was used is slower than most relevant

time-varying human behavior (∼1–2 Hz, e.g., human walking). The simulations of the time-varying stiffness according to a square wave demonstrate that the skirt decomposition method is unable to capture rapid time-variations in the presence of noise using the current design of the multisine perturbation signal. It will require optimization of the multisine perturbation signal to provide greater space between excited frequencies. Considering the limited bandwidth of human joints this may be difficult.

Likewise, the KBR does not seem to perform well for estimating rapid transitions in joint stiffness. However, this is inherent to the use of the radial basis function kernel and the choice of the values for the hyperparameters, optimized to capture the 0.05 Hz expected time-variance in joint stiffness. Hence, this results in smoothing of any rapid changes in joint stiffness and minimizes the effects of noise on the estimate (visible in Fig. 3)-which benefits the estimate compared to the skirt decomposition method (Table I). To some extent, the hyperparameters dictate the time-variance that can be captured. Preliminary simulations have demonstrated that the KBR method can identify rapid time-variations by optimizing its hyperparameters or choosing a different basis function. However, this will result in a model of higher complexity, and therefore higher uncertainty as there is a greater risk of modeling noise. Future work will have to establish the exact possibilities and constraints of both methods for identifying time-varying joint impedance.

C. Time-Varying Human Joint Impedance

Observing a time-varying joint stiffness and resonance frequency when varying the level of torque is in line with earlier reports [7], [9], [49]. An increasing resonance frequency, accompanied with an increase in joint stiffness, was reported for the ankle joint when generating a torque by pushing the foot down (i.e., plantarflexion) [9]. The KBR method demonstrates a similar sinusoidal pattern in joint stiffness. Impedance is high when torque is high, and vice versa. For the skirt method, this distinction is less clear. This may be partly attributed to the frequency resolution inherent to the nonparametric skirt method.

The KBR method [Fig. 8(b)] also reveals a change in the size of the peak at the resonance frequency. This peak is larger for higher levels of torque, which may be attributed to the underlying mechanisms that allow humans to successfully complete the requested motor task. Humans can adapt the mechanical behavior of their joints by regulating intrinsic and reflexive joint properties [1], [50]. Intrinsic properties can be tuned by cocontracting, i.e., activating different muscles that act in opposite directions around a joint at the same time results in increased joint impedance. This is primarily expressed in a change in intrinsic stiffness, which has a greater sensitivity for muscle activation than intrinsic viscosity [7], [49]. Whereas intrinsic properties are primarily tuned feedforward, an adaptation of reflex properties involves feedback pathways with an inherent time delay resulting in phase lags [51]. An increase in voluntary torque level up to 20% MVT has been demonstrated to raise the contribution of both the intrinsic and reflexive stiffness [7], [35]. As a result of the larger reflexive contribution and involved time delay, oscillatory behavior at the resonance frequency is increased. Whereas this is one explanation for the increased resonance peak when the voluntary torque is increased to 20% MVT, it may also simply reflect the changing muscle viscoelastic properties with increasing levels of muscle activation. The currently employed identification technique does not yet allow for separation of intrinsic and reflexive contributions to the motor behavior but this is work in progress. This could, for example, be done by fitting a parametric model to the TV-FRFs so to extract these detailed parameters that determine joint impedance [1].

VII. Conclusion

This paper presents a novel framework for the identification of time-varying joint impedance by making use of two different LTV SI methods. Both the parametric KBR method and the nonparametric skirt method allow identification of joint impedance over time using a single trial of data. Despite the low SNR of the recorded signals in the biomedical domain, there is the possibility to successfully quantify changes in joint impedance over time based on limited data. In the future, this may allow gaining valuable new insights into how humans control their limbs and learn new tasks. The successful application of SI methods, unknown in the biomedical domain, demonstrates that cross domain collaborations are important to make full use of all that the field of SI has to offer in studying human control behavior.

Appendix

A. Skirt Decomposition Method

This appendix summarizes the algorithm for the skirt decomposition method, which is proposed in [37]. The model in (7) is approximated in a frequency band comprising three successive excited frequencies, denoted k_{e}^{-}, k_{e}, and k_{e}^{+}, as

$$Y_m(k) \approx \frac{1}{N} \sum_{p=0}^{N_p} \sum_{k' \in \{k_{\mathrm{e}}^{-}, k_{\mathrm{e}}, k_{\mathrm{e}}^{+}\}} G_p(j\omega_{k'}) U(k') \ldots B_p(k-k') + I_Y(j\omega_k) \quad \text{(A.1)}$$

expressed in the frequencies $k = k_e^{-} - \Delta_{k_e}, \ldots, k_e^{+} + \Delta_{k_e}$ with

$$I_Y(k) = \sum_{n=0}^{N_{\mathrm{r}}} r_n k^n \quad \text{(A.2)}$$

a polynomial in k, which captures $T_Y(j\omega_k)$ and the fact that only a limited number of terms from (7) are included in (A.1), $\Delta_{k_{\mathrm{e}}}$ is the distance (in bins) between two excited frequencies. By solving (A.1) for $G_p(j\omega_{k'})$ and r_n in least squares sense, for all $k_e \epsilon K_{exc}$, the LTI blocks G_p are effectively estimated nonparametrically (i.e., at the excited frequencies only) in a sliding frequency band. Note that (A.1) is linear in all the unknowns [$G_p(j\omega_{k'})$ and r_n].

B. Kernel-Based Regression Method

This appendix summarizes the algorithm for the KBR method, which is proposed in [39]. The estimate is defined as

$$\hat{a}_n, \hat{b}_n = \underset{a_n, b_n}{\operatorname{argmin}} \sum_{k \in \mathrm{K_{int}}} \frac{|E(k, a_n, b_n)|^2}{\hat{\sigma}_E^2(k, a_n, b_n)} \cdots + \sum_{n=1}^{N_a} \breve{a}_n^T K^{-1} \breve{a}_n + \sum_{n=0}^{N_b} \breve{b}_n^T K^{-1} \breve{b}_n \quad \text{(B.1)}$$

with

$$E(k, a_n, b_n) = \mathrm{DFT}\left\{ y - \sum_{n=0}^{N_b} b_n u^{(n)} + \sum_{n=1}^{N_a} a_n y^{(n)} \right\}_k$$
$$a_n = \mathring{a}_n + \breve{a}_n, b_n = \mathring{b}_n + \breve{b}_n \quad \text{(B.2)}$$

where a_n and b_n are vectorised versions of $a_n(t)$ and $b_n(t)$ in $t = 0, T_s, \ldots, (N-1)T_s$, $u^{(n)}$ and $y^{(n)}$ are the sampled and vectorised nth derivatives of $u(t)$ and $y(t)$. The parameters a_n and b_n are decomposed into $\mathring{a}_n$ and $\mathring{b}_n$ (which are constant vectors to which no regularization is applied) and $\breve{a}_n$ and $\breve{b}_n$ (which are the time-varying and regularized to impose their smoothness). The latter is done by including the sums of $\breve{a}_n^T K^{-1} \breve{a}_n$ and $\breve{b}_n^T K^{-1} \breve{b}_n$. The kernel matrix K is semipositive definite and symmetric, and imposes structure on the estimated parameters.

σ_E^2 is the variance of E. Explicit expressions for E and σ_E^2, based on the sampled signals $u(t)$ and $y(t)$ are available in [39].

Note that (B.2) is a nonquadratic (and in general nonconvex) problem, due to the division by $\hat{\sigma}_E^2$. This is solved via an iterative convex relaxation, where $\hat{\sigma}_E^2$ is initialized to 1 and, for the mth iteration, is computed as $\hat{\sigma}_{E,m}^2(k) \leftarrow \hat{\sigma}_E^2(k, \hat{a}_{n,m-1}, \hat{b}_{n,m-1})$, with $\hat{a}_{n,m-1}, \hat{b}_{n,m-1}$ the estimates obtained at the $(m-1)$th iteration. This algorithm is outlined in [39, Sec. 6.2]. The computation of $\hat{\sigma}_E^2$ also requires an estimate of the noise variance on the measured spectra, which is computed via the method presented in [52].

Note that this estimator does not require the explicit computation of K^{-1}. This allows for the use of (close to) singular kernel matrices.

REFERENCES

[1] F. C. T. van der Helm, A. C. Schouten, E. de Vlugt, and G. G. Brouwn, "Identification of intrinsic and reflexive components of human arm dynamics during postural control," (in English), *J. Neurosci. Methods*, vol. 119, no. 1, pp. 1–14, Sep. 2002.

[2] E. Todorov, "Optimality principles in sensorimotor control," *Nature Neurosci.*, vol. 7, no. 9, pp. 907–915, Sep. 2004.

[3] E. J. Perreault, R. F. Kirsch, and P. E. Crago, "Multijoint dynamics and postural stability of the human arm," (in English), *Exp. Brain Res.*, vol. 157, no. 4, pp. 507–517, Aug. 2004.

[4] D. Ludvig and E. J. Perreault, "System identification of physiological systems using short data segments," (in English), *IEEE Trans. Biomed. Eng.*, vol. 59, no. 12, pp. 3541–3549, Dec. 2012.

[5] D. Ludvig, E. J. Perreault, and R. E. Kearney, "Efficient estimation of time-varying intrinsic and reflex stiffness," (in English), in *Proc. IEEE Annu. Int. Conf. Eng. Med. Biol. Soc.*, Aug./Sep. 2011, pp. 4124–4127.

[6] D. Ludvig, I. Cathers, and R. E. Kearney, "Voluntary modulation of human stretch reflexes," (in English), *Exp. Brain Res.*, vol. 183, no. 2, pp. 201–213, Nov. 2007.

[7] M. M. Mirbagheri, H. Barbeau, and R. E. Kearney, "Intrinsic and reflex contributions to human ankle stiffness: Variation with activation level and position," *Exp. Brain Res.*, vol. 135, no. 4, pp. 423–436, Dec. 2000.

[8] R. E. Kearney and I. W. Hunter, "Dynamics of human ankle stiffness: Variation with displacement amplitude," *J. Biomech.*, vol. 15, no. 10, pp. 753–756, 1982.

[9] I. W. Hunter and R. E. Kearney, "Dynamics of human ankle stiffness: Variation with mean ankle torque," *J. Biomech.*, vol. 15, no. 10, pp. 747–752, 1982.

[10] R. M. Enoka and J. Duchateau, "Muscle fatigue: What, why and how it influences muscle function," *J. Physiol.*, vol. 586, no. 1, pp. 11–23, Jan. 2008.

[11] Y. van Ingelgem, E. Tourwé, J. Vereecken, and A. Hubin, "Application of multisine impedance spectroscopy, FE-AES and FE-SEM to study the early stages of copper corrosion," *Electrochim. Acta*, vol. 53, no. 25, pp. 7523–7530, 2008.

[12] G. F. Sirca, Jr., and H. Adeli, "System identification in structural engineering," *Sci. Iranica*, vol. 19, no. 6, pp. 1355–1364, 2012.

[13] M. D. Spiridonakos and S. D. Fassois, "Parametric identification of a time-varying structure based on vector vibration response measurements," *Mech. Syst. Signal Process.*, vol. 23, no. 6, pp. 2029–2048, 2009.

[14] J. Ertveldt, J. Lataire, R. Pintelon, and S. Vanlanduit, "Frequency-domain identification of time-varying systems for analysis and prediction of aeroelastic flutter," *Mech. Syst. Signal Process.*, vol. 47, nos. 1–2, pp. 225–242, 2014.

[15] J. Lataire and R. Pintelon, "Frequency-domain weighted non-linear least-squares estimation of continuous-time, time-varying systems," *IET Control Theory Appl.*, vol. 5, no. 7, pp. 923–933, May 2011.

[16] P. Z. Csurcsia and J. Lataire, "Nonparametric estimation of time-varying systems using 2-D regularization," *IEEE Trans. Instrum. Meas.*, vol. 65, no. 5, pp. 1259–1270, May 2016.

[17] R. Zou and K. H. Chon, "Robust algorithm for estimation of time-varying transfer functions," (in English), *IEEE Trans. Biomed. Eng.*, vol. 51, no. 2, pp. 219–228, Feb. 2004.

[18] J. K. Hammond and P. R. White, "The analysis of non-stationary signals using time-frequency methods," *J. Sound Vibrat.*, vol. 190, no. 3, pp. 419–447, Feb. 1996.

[19] W. J. Staszewski and D. M. Wallace, "Wavelet-based frequency response function for time-variant systems—An exploratory study," *Mech. Syst. Signal Process.*, vol. 47, nos. 1–2, pp. 35–49, 2014.

[20] S. Conforto and T. D'Alessio, "Spectral analysis for non-stationary signals from mechanical measurements: A parametric approach," *Mech. Syst. Signal Process.*, vol. 13, no. 3, pp. 395–411, 1999.

[21] R. Pintelon and J. Schoukens, *System Identification: A Frequency Domain Approach*. Hoboken, NJ, USA: Wiley, 2012.

[22] T. E. Sobhani, K. Jalaleddini, and R. E. Kearney, "Linear parameter varying identification of ankle joint intrinsic stiffness during imposed walking movements," (in English), in *Proc. IEEE 35th Annu. Int. Conf. Eng. Med. Biol. Soc. (EMBC)*, Jul. 2013, pp. 4923–4927.

[23] R. B. Stein and R. E. Kearney, "Nonlinear behavior of muscle reflexes at the human ankle joint," *J. Neurophysiol.*, vol. 73, no. 1, pp. 65–72, Jan. 1995.

[24] R. F. Kirsch and R. E. Kearney, "Identification of time-varying stiffness dynamics of the human ankle joint during an imposed movement," *Experim. Brain Res.*, vol. 114, no. 1, pp. 71–85, Mar. 1997.

[25] D. J. Bennett, J. M. Hollerbach, Y. Xu, and I. W. Hunter, "Time-varying stiffness of human elbow joint during cyclic voluntary movement," *Exp. Brain Res.*, vol. 88, no. 2, pp. 433–442, 1992.

[26] H. Lee and N. Hogan, "Time-varying ankle mechanical impedance during human locomotion," (in English), *IEEE Trans. Neural Syst. Rehabil. Eng.*, vol. 23, no. 5, pp. 755–764, Sep. 2015.

[27] D. Ludvig, M. Plocharski, P. Plocharski, and E. J. Perreault, "Mechanisms contributing to reduced knee stiffness during movement," (in English), *Exp. Brain Res.*, vol. 235, no. 10, pp. 2959–2970, Oct. 2017.

[28] H. I. Giesbrecht, M. Baker, D. Ludvig, R. Wagner, and R. E. Kearney, "Identification of time-varying intrinsic and reflex joint stiffness," (in English), *IEEE Trans. Biomed. Eng.*, vol. 58, no. 6, pp. 1715–1723, Jun. 2011.

[29] J. B. MacNeil, R. E. Kearney, and I. W. Hunter, "Identification of time-varying biological systems from ensemble data (joint dynamics application)," *IEEE Trans. Biomed. Eng.*, vol. 39, no. 12, pp. 1213–1225, Dec. 1992.

[30] J. F. Soechting, J. R. Dufresne, and F. Lacquaniti, "Time-varying properties of myotatic response in man during some simple motor tasks," *J. Neurophysiol.*, vol. 46, no. 6, pp. 1226–1243, Dec. 1981.
[31] M. Mulder *et al.*, "Identification of time variant neuromuscular admittance using wavelets," (in English), in *Proc. IEEE Int. Conf. Syst., Man, Cybern. (SMC)*, Oct. 2011, pp. 1474–1480.
[32] M. P. Vlaar, T. Solis-Escalante, A. N. Vardy, F. C. T. van der Helm, and A. C. Schouten, "Quantifying nonlinear contributions to cortical responses evoked by continuous wrist manipulation," *IEEE Trans. Neural Syst. Rehabil. Eng.*, vol. 25, no. 5, pp. 481–491, May 2017.
[33] C. M. Harris and D. M. Wolpert, "Signal-dependent noise determines motor planning," *Nature*, vol. 394, no. 6695, pp. 780–784, Aug. 1998.
[34] S. H. Scott and G. E. Loeb, "The computation of position sense from spindles in mono- and multiarticular muscles," *J. Neurosci.*, vol. 14, no. 12, pp. 7529–7540, Dec. 1994.
[35] M. A. Golkar, T. E. Sobhani, and R. E. Kearney, "Linear parameter varying identification of dynamic joint stiffness during time-varying voluntary contractions," (in English), *Frontiers Comput. Neurosci.*, vol. 11, p. 35, May 2017.
[36] D. L. Guarin and R. E. Kearney, "Time-varying identification of ankle dynamic joint stiffness during movement with constant muscle activation," in *Proc. IEEE 37th Annu. Int. Conf. Eng. Med. Biol. Soc. (EMBC)*, Aug. 2015, pp. 6740–6743.
[37] J. Lataire, R. Pintelon, and E. Louarroudi, "Non-parametric estimate of the system function of a time-varying system," *Automatica*, vol. 48, no. 4, pp. 666–672, Apr. 2012.
[38] L. A. Zadeh, "Frequency analysis of variable networks," *Proc. IRE*, vol. 38, no. 3, pp. 291–299, Mar. 1950.
[39] J. Lataire, R. Pintelon, D. Piga, and R. Tóth, "Continuous-time linear time-varying system identification with a frequency-domain kernel-based estimator," (in English), *IET Control Theory Appl.*, vol. 11, no. 4, pp. 457–465, Feb. 2017.
[40] A. C. Schouten, E. de Vlught, and F. C. T. van der Helm, "Quantification of spinal reflexes in neurological disorders," in *Proc. IEEE Int. Conf. Syst., Man Cybern.*, vol. 3, Oct. 2004, pp. 2492–2499.
[41] J. Lataire, E. Louarroudi, and R. Pintelon, "Detecting a time-varying behavior in frequency response function measurements," *IEEE Trans. Instrum. Meas.*, vol. 61, no. 8, pp. 2132–2143, Aug. 2012.
[42] R. Pintelon, E. Louarroudi, and J. Lataire, "Nonparametric time-variant frequency response function estimates using arbitrary excitations," *Automatica*, vol. 51, no. 1, pp. 308–317, 2015.
[43] A. C. Schouten, E. de Vlugt, J. J. van Hilten, and F. C. van der Helm, "Design of a torque-controlled manipulator to analyse the admittance of the wrist joint," (in English), *J. Neurosci. Methods*, vol. 154, nos. 1–2, pp. 134–141, Jun. 2006.
[44] D. Ludvig and E. J. Perreault, "Estimation of joint impedance using short data segments," in *Proc. Conf. IEEE Eng. Med. Biol. Soc.*, vol. 2011, Aug. 2011, pp. 4120–4123.
[45] D. L. Guarin and R. E. Kearney, "Estimation of time-varying, intrinsic and reflex dynamic joint stiffness during movement. Application to the ankle joint," (in English), *Frontiers Comput. Neurosci.*, vol. 11, p. 51, Jun. 2017.
[46] J.-W. van Wingerden and M. Verhaegen, "Subspace identification of Bilinear and LPV systems for open- and closed-loop data," *Automatica*, vol. 45, no. 2, pp. 372–381, 2009.
[47] T. E. Sobhani, K. Jalaleddini, and R. E. Kearney, "Ankle joint intrinsic dynamics is more complex than a mass-spring-damper model," (in English), *IEEE Trans. Neural Syst. Rehabil. Eng.*, vol. 25, no. 9, pp. 1568–1580, Sep. 2017.
[48] J. Lataire, D. Piga, and R. Tóth, "Frequency-domain least-squares support vector machines to deal with correlated errors when identifying linear time-varying systems," *IFAC Proc. Volumes*, vol. 47, no. 3, pp. 10024–10029, 2014.
[49] P. L. Weiss, I. W. Hunter, and R. E. Kearney, "Human ankle joint stiffness over the full range of muscle activation levels," *J. Biomech.*, vol. 21, no. 7, pp. 539–544, 1988.
[50] T. R. Nichols and J. C. Houk, "Improvement in linearity and regulation of stiffness that results from actions of stretch reflex," (in English), *J. Neurophysiol.*, vol. 39, no. 1, pp. 119–142, Jan. 1976.
[51] A. C. Schouten, E. de Vlugt, J. J. van Hilten, and F. C. van der Helm, "Quantifying proprioceptive reflexes during position control of the human arm," (in English), *IEEE Trans. Biomed. Eng.*, vol. 55, no. 1, pp. 311–321, Jan. 2008.
[52] J. Lataire and R. Pintelon, "Estimating a nonparametric colored-noise model for linear slowly time-varying systems," *IEEE Trans. Instrum. Meas.*, vol. 58, no. 5, pp. 1535–1545, May 2009.

Mark van de Ruit received the M.Sc. degree in biomedical engineering from the Delft University of Technology, Delft, The Netherlands, in 2011, and the Ph.D. degree in neurophysiology from the University of Birmingham, Birmingham, U.K., in 2016.

He is currently a Post-Doctoral Researcher with the Delft University of Technology. His current research is in neuromuscular control, combing electrophysiological recording techniques with system identification to obtain a better understanding of human motion control in healthy individuals and those suffering of movement disorders.

Gaia Cavallo (S'18) received the M.Sc. degree (*cum laude*) in systems and control and biomedical engineering from the Delft University of Technology, Delft, The Netherlands, in 2017. She is currently pursuing the Ph.D. degree with the Department of ELEC, Vrije Universiteit Brussel, Brussels, Belgium.

Her current research interests include system identification of biomedical applications.

John Lataire (S'06–M'11) was born in Brussels, Belgium, in 1983. He received the Electrical Engineer degree in electronics and information processing and the Ph.D. degree in engineering sciences from Vrije Universiteit Brussel, Brussels, in 2006 and 2011, respectively.

He is currently with the Department of ELEC, Vrije Universiteit Brussel, where he was involved in the identification of dynamic systems, especially on time-varying systems, and the use of kernel-based regression in system identification.

Dr. Lataire was a recipient of the 2008 IOP Outstanding Paper Award (best paper in Measurement Science and Technology), the Andy Chi Award for the best paper in IEEE TRANSACTION ON INSTRUMENTATION AND MEASUREMENT in 2014, and the J. Barry Oakes Advancement Award from the IEEE INSTRUMENTATION AND MEASUREMENT SOCIETY in 2016.

Frans C. T. van der Helm received the M.Sc. degree in human movement science and the Ph.D. degree (*cum laude*) in mechanical engineering from the Delft University of Technology, Delft, The Netherlands, in 1985 and 1991, respectively.

He is currently a Professor of biomechatronics and biorobotics with the Delft University of Technology, and an Adjunct Professor with the University of Twente, Enschede, The Netherlands, and Northwestern University, Evanston, IL, USA. He is one of the Program Leaders in the Medical Delta, and NeuroCIMT Program. He received an ERC Advanced Grant on 4-D EEG: A new tool to assess the spatial and temporal activity in the cortex. His current research interests include biomechanics of the upper and lower extremity, neuromuscular control, eye biomechanics, pelvic floor biomechanics, human motion control, and posture stability.

Winfred Mugge received the M.Sc. and Ph.D. degrees in mechanical engineering from the Delft University of Technology, CD Delft, The Netherlands, in 2006 and 2011, respectively.

He is currently an Assistant Professor with the Delft University of Technology. His research interests include human motor control, neuromechanics, haptics, system identification, and orthotics.

Jan-Willem van Wingerden was born in Ridderkerk, The Netherlands, in 1980. He received the B.S. and Ph.D. (*cum laude*) degrees from the Delft Center for Systems and Control, Delft University of Technology, Delft, The Netherlands, in 2004 and 2008, respectively. His Ph.D. thesis was entitled Smart Dynamic Rotor Control for Large Offshore Wind Turbines.

He is currently a Professor with the Delft University of Technology. His current research interests include linear parameter varying identification, subspace identification, smart structures and control, and identification of wind turbines and wind farms.

Alfred C. Schouten received the M.Sc. and Ph.D. degrees in mechanical engineering from Delft University of Technology, Delft, The Netherlands, in 1999 and 2004, respectively.

He is currently an Associate Professor with the Delft University of Technology and the University of Twente, Enschede, The Netherlands, and a Cofounder of the Delft Laboratory for Neuromuscular Control, Delft University of Technology. His current research interests include the field of neuromuscular control, neuromuscular modeling, haptic manipulators, and system identification.